

Quadrupole splittings in the near-infrared spectrum of $^{14}\text{NH}_3$

Sylvestre Twagirayezu,^{1, a)} Gregory E. Hall,^{1, b)} and Trevor J. Sears^{1, 2, c)}

¹⁾*Division of Chemistry, Department of Energy and Photon Sciences, Brookhaven National Laboratory, Upton, NY 11973-5000, USA*

²⁾*Chemistry Department, Stony Brook University, Stony Brook, NY 11794, USA*

(Dated: 20 September 2022)

Sub-Doppler, saturation dip, spectra of lines in the $v_1 + v_3$, $v_1 + 2v_4$ and $v_3 + 2v_4$ bands of $^{14}\text{NH}_3$ have been measured by frequency comb-referenced diode laser absorption spectroscopy. The observed spectral line widths are dominated by transit time broadening, but show resolved or partially-resolved hyperfine splittings that are primarily determined by the ^{14}N quadrupole coupling. Modeling of the observed line shapes based on the known hyperfine level structure of the ground state of the molecule shows that, in nearly all cases, the excited state level has hyperfine splittings similar to the same rotational level in the ground state. The data provide accurate frequencies for the line positions and easily separate lines overlapped in Doppler-limited spectra. The observed hyperfine splittings can be used to make and confirm rotational assignments and ground state combination differences obtained from the measured frequencies are comparable in accuracy to those obtained from conventional microwave spectroscopy. One upper state level shows very clear differences from the expected splittings. Examination of the known vibration-rotation level structure shows there is a near degeneracy between this level in $v_1 + v_3$ and a rotational level in the $v_1 + 2v_4$ manifold which is of the appropriate symmetry to be mixed by magnetic hyperfine terms that couple ortho- and para- forms of the molecule.

^{a)}Electronic mail: sylvestret@bnl.gov

^{b)}Electronic mail: gehall@bnl.gov

^{c)}Electronic mail: sears@bnl.gov, trevor.sears@stonybrook.edu

I. INTRODUCTION

Ammonia, NH_3 , is a symmetric top rotor possessing a large amplitude inversion vibrational mode. The inversion motion is associated with a double-well potential¹ with an effective barrier height of 2020 cm^{-1} . Tunneling through the barrier leads to the well-known inversion splittings^{1,2} in the zero point, and higher, levels of the molecule. Further, the spins of the three equivalent protons result in two nuclear spin states of the molecule, ortho- ($\mathbf{I_H} = 3/2$) and para- ($\mathbf{I_H} = 1/2$) each associated with a distinct set of rotational levels.³ The two sets of levels do not interact under most circumstances. These characteristics, together with its practical importance, have made ammonia a prototype molecule for spectroscopic studies.

There has been considerable published work on the near-infrared spectrum of ammonia during the past few years.^{4–11} The spectrum in this region consists of a mixture of combination and overtone bands, of which the perpendicular bands $v_1 + v_3$, $v_1 + 2v_4$, $v_3 + 2v_4$, $2v_1$, and $2v_3$ are the most prominent. However, despite many years of work, the spectroscopic analysis remains incomplete because of the many overlapping rotational features, (at Doppler-limited resolution), multiple uncharacterized perturbations caused by anharmonic and Coriolis mixing, and the presence of hot band lines in the low-frequency inversion mode. The great majority of the observed features in recent high resolution measurements in the near-infrared remain rotationally unassigned.^{4,5} Isotopically labeled samples¹² permitted more solid assignments of some of the strongest feature of NH_3 but again leave many features unassigned. Variable (low) temperature studies⁶ of the spectrum have led to the assignment of the lower state energies for many of the spectroscopic features and have permitted further assignments and corrections to earlier ones. Very recently, the Tennyson group⁷ have critically reviewed and validated all the available high resolution spectroscopic data for ammonia, to create a database of known levels and band origins. Combined with previously calculated absorption intensities, this work provides a detailed and accurate map of the assigned spectrum of ammonia from the microwave through the near-infrared. The work resulted in a Measured Active Rotational-Vibrational Energy Levels (MARVEL) database that can be dynamically updated as new data become available.

In the present work, we report sub-Doppler measurements of a number of transitions in the $v_1 + v_3$, $v_1 + 2v_4$ and $v_3 + 2v_4$ bands. These measurements fully resolve many over-

lapped vibration-rotation features in the Doppler-limited spectra whose presence have previously hindered assignments.¹² The new measurements also exhibit partially resolved nuclear hyperfine structure due to the ¹⁴N quadrupole and proton hyperfine couplings. The observed hyperfine patterns are spectroscopic signatures of the rotational levels involved in the transitions^{13–16} and may therefore be used to confirm or deny spectroscopic assignments. Czajkowski et al.¹⁰ have previously reported the measurement of a few sub-Doppler lines in the ammonia spectrum in this region, but did not report the observation of quadrupole structure, presumably because the measurements were conducted at higher pressures than the current work, resulting in some collisional broadening.

One transition observed, the $v_1 + v_3$, ³ $P(5, 4)_a$ transition at 6537.6806 cm^{−1}, frequency measured here at 195 994.734 57(2) GHz, exhibits hyperfine structure which does not conform to that expected based on the assumption that the known lower state hyperfine splittings¹⁶ do not change on vibrational excitation. Based on extensive previous Doppler-limited spectroscopic measurements^{4,7} there seems little doubt that the spectroscopic assignment is secure. Hence, the observed change in the quadrupole splitting must be due to a perturbation in the upper level, *i.e.* (4, 3)_a of ($v_1 + v_3$). Examination of the upper energy levels listed in the MARVEL database,⁷ shows that this level is very close in energy to (5, 4)_s of the $v_1 + 2v_4$ vibrational level. Interestingly, (4, 3)_a of ($v_1 + v_3$) belongs to the para- set of proton hyperfine levels,³ while (5, 4)_s of $v_1 + 2v_4$ is an ortho- level. Close study of the database shows that, in this region, this pair of levels is the only one known to occur where a near degeneracy between levels has the appropriate symmetry for ortho-para mixing to occur, raising the intriguing possibility that it is the coupling associated with the observed perturbed hyperfine pattern.

II. EXPERIMENTAL METHODS

The spectrometer used in this work has been described in detail previously.¹⁷ Samples of anhydrous ammonia gas (Matheson Gas, Inc.) were introduced in the cavity-type absorption cell at pressures of between 1 and 20 mTorr (0.133-2.66 Pa) depending on the strength of the absorption. Sub-Doppler, saturation dip, spectra of rotational lines in the ammonia spectrum near 1.5 μ m were recorded. Some collisional broadening of the saturation features could be observed at higher pressures, but no attempt was made to quantify this effect in

this work. As in previous work,¹⁷ the stronger saturation dip features could also be power-broadened and distorted at higher laser powers. Therefore, spectra were recorded at the lowest pressure and laser power consistent with satisfactory signal-to-noise ratios. Examples of observed derivative signals of the saturation dip profiles are shown in Figures 1 and 2. These were obtained by scanning the comb repetition rate by 0.25 Hz/step, corresponding to approximately 60 kHz/step in the optical frequency across the saturation dip, typically collecting an averaged signal for 3 seconds at each frequency step. A few weaker lines required more averaging to obtain satisfactory signal-to-noise ratios.

III. RESULTS AND ANALYSIS

The measured frequencies are given in Table I. All the measured saturation dip transitions showed either resolved splittings or distortions in the line shape compared to a derivative of a single Lorentzian transmission lineshape.¹⁸ Individual line widths are dominated by transit-time broadening¹⁷ and the lineshapes arise from partially resolved hyperfine splittings which are dominated by nuclear quadrupole couplings due to the ¹⁴N nucleus, $\mathbf{I}_N = \mathbf{1}$, that, in all but the lowest rotational levels, result in a splitting of each rotational level (J) into three sub-levels labeled here by the quantum number F_1 , $F_1 = J, J \pm 1$. Superimposed on the quadrupole structure, each level is further split by the proton nuclear hyperfine structure due to the ¹H nuclear spin-rotation coupling and nuclear spin-spin dipolar coupling. The three equivalent protons lead to ortho- ($\mathbf{I}_H = 3/2$) and para- ($\mathbf{I}_H = 1/2$) proton nuclear spin functions,³ and the total angular momentum is $\mathbf{F} = \mathbf{F}_1 + \mathbf{I}_H$, quantum number F . Measurements by Kukolich^{13–15} and additional analysis by Hougen¹⁶ fully characterized the hyperfine structure in the lowest inversion doublet ($v_2 = 0$) of the ¹⁴NH₃ molecule. The proton hyperfine splittings are less than a few tens of kHz, too small to be resolved in the current experiments. The quadrupole coupling energy contributions are determined by the matrix elements:^{13,16}

$$W_Q(F_1, J, K) = (-1)^{J+I_N+F_1} \left\{ \begin{array}{ccc} F_1 & I_N & J' \\ 2 & J & I_N \end{array} \right\} \langle J' | V | J K \rangle \langle I_N || Q || I_N \rangle \quad (1)$$

where V and Q are matrix elements which depend on J , K and I_N . The V contribution is:

$$\langle J' K | V | J K \rangle = \frac{1}{2} q [(2J' + 1)(2J + 1)]^{1/2} (-1)^{J'+K} \begin{pmatrix} J' & 2 & J \\ -K & 0 & K \end{pmatrix} \quad (2)$$

and Q :

$$\langle I_N || Q || I_N \rangle = \frac{1}{2} eQ(2I_N + 1) \left[\frac{(2I_N + 3)(I_N + 1)}{I_N(2I_N - 1)(2I_N + 1)} \right]^{1/2} \quad (3)$$

The energy contributions from matrix elements off-diagonal in J are negligible compared to the experimental resolution here, so we computed just the diagonal contributions to the quadrupolar splittings in simulating the observed spectral features *i.e.* $J'=J$ in eq. (1) above. These expressions were used to calculate the quadrupolar hyperfine splittings for each rotational level of interest. Also, although the inversion doublet levels have slightly different quadrupolar splittings, determined by the parameter ΔQ^* in Hougen's notation,¹⁶ these differences are small compared to the current experimental measurement precision, so they too were neglected. The calculated ¹⁴N quadrupole splittings based on this model for the rotational levels in NH₃ of interest here are given in Table II.

Spectroscopic transitions and are expected to obey the selection rules, $\Delta F_1 = 0, \pm 1$ and the observed line shapes were modeled as a convolution of Lorentzian derivatives¹⁸ for each possible quadrupolar hyperfine transition as detailed below. Relative intensities of the quadrupole split transitions are given by:

$$\text{Intensity}_Q(\text{rel.}) = \left[(-1)^{J'+F'_1} [(2F'_1 + 1)(2F_1 + 1)]^{1/2} \begin{Bmatrix} I_N & J' & F'_1 \\ I_N & F_1 & J \end{Bmatrix} \right]^2 \quad (4)$$

With the aid of eq.(1) and eq.(4), the observed lineshapes were modeled in steps: (i) the quadrupole energy level patterns for the rotational levels involved in the transition were estimated using the known microwave parameters;¹⁶ (ii) the component quadrupole transition frequencies were then estimated by subtracting the lower energy levels ($W_Q(F_1, J, K)$) from the upper split levels ($W_Q(F'_1, J', K')$) with the selection rules, $\Delta F_1 = 0, \pm 1$, and the relative intensities computed from eq. (4). Finally, these component frequency offsets and relative intensities were used to create a line shape as the first derivative of a Lorentzian¹⁸ of width (HWHM) 290 kHz, to account for transit time and other broadening. The individual component profiles were summed to give a composite line shape to compare to the experimental trace. Lines recorded at higher pressures (>5 mT) were broader and modeled

by appropriately adjusting the empirical width parameter. The calculated profile was then manually frequency offset to overlay the frequency of the observed feature which is thus determined by a central frequency (ν_0) and a set of quadrupolar component offsets, ΔW_Q . The predicted line shapes were in good accord with the observations, with the exception of the ${}^pP(5, 4)_a$ transition discussed in more detail below. The predictions could be refined by slightly adjusting the estimated quadrupolar shifts (ΔW_Q) for the component transitions by applying small changes to the upper, quadrupole split, energy levels while keeping ground state splittings fixed, but this was not carried out for the majority of the observations because assuming the quadrupole parameters do not change on vibrational excitation resulted in predicted line shapes that were close to those observed. Figure (1) illustrates the results of this procedure for the ${}^rP(3, 0)_s$ transition at 196 193.824 GHz^{4,7} while Figure (2) illustrates the more complex line shapes observed for some of the lower- J transitions. For all but the lowest J transitions, the intensity of the strongly allowed $\Delta F_1 = \Delta J$ components dominate the observed line shape. Figure (3) shows examples of a series of transitions from levels with $J = 5$. The lines shown on these spectra are the calculated profiles following refinement of the quadrupole splittings by adjustment of the upper level quadrupole splitting. The difference between the ${}^pP(5, 4)$ a and s components is noteworthy. In the model, the two should have identical shapes, and the observations for the $K = 5$ and $K = 3$ transitions match this expectation

All the frequency measured lines were modeled and estimated line center frequencies extracted. The results are summarized in Table I. The frequency for the line center is not necessarily exactly the hyperfine-free frequency since the hyperfine splittings were not fully resolved and the modeling is approximate. In the modeling to determine the line centers, the observed and calculated zero-crossing positions were matched. Thus any model errors result in inaccuracy in the reported line center. These errors are of the same order of magnitude as errors expected from the neglect of the proton hyperfine and other neglected contributions to the line shape and close to the experimental resolution. For this reason, we report a conservative estimate of the line center measurement errors as ± 20 kHz for most of the data. Exceptions are noted in table I when the lines were weak and/or for transitions where the observed quadrupole splitting patterns were complicated, typically low- J transitions. The accuracy of the measurement of the position of the zero-crossing of an observed line shape is actually better than this, and of the order of 3-10 kHz.¹⁷

The modeling of the observed ${}^pP(5,4)_a$ line shape requires large changes from the expected quadrupole splittings in the upper level as shown in Figure (4). While patterns for all other measured transitions closely conform to those calculated using the known ground state parameters, the pattern for this transition is significantly different. Fig. (4)(b) shows the upper energy splittings (F') in this transition are substantially quenched leading to shifts of -410 kHz, 20 kHz, and 200 kHz between the $F_1 = J, J \pm 1$ transitions, respectively.

Absolute frequencies given in Table I are generally within the estimated errors of those reported by Sung *et al.*⁴ and Földes *et al.*⁶ when allowing for the fact that many of the new measurements are of components of overlapped features in the Doppler-limited spectra. The accuracy and precision of the present measurements places much tighter constraints on ground state combination differences in the ammonia spectrum in this region.

The frequency coverage of the spectrometer currently prevents measurements at frequencies of 199 THz and higher, but the present data permit the determination of five ground state combination differences. These are given in Table III where they are also compared to numbers derived from the published energy levels¹⁹ derived from microwave and near infrared data for the lowest inversion doublet levels. Comparison shows that the present energy differences are systematically somewhat larger than those derived from the published data, with the differences increasing with rotational energy. Even so, the largest deviations are less than 1 MHz, however, and unresolved hyperfine splittings in the earlier data could be the major contributor to the differences. Future modifications to the current spectrometer will permit many more combination differences to be determined in these vibrational bands, and a significant improvement in the accuracy of the rotational energy levels of ammonia could result from such measurements.

IV. DISCUSSION AND CONCLUSIONS

The new data illustrate the precision that can be obtained from sub-Doppler measurements in the near-infrared. The data provide accurate rest frequencies for transitions that are overlapped in the best Doppler-limited spectra and can resolve ambiguities in spectral assignments. The precision of lower state energy level combination differences derived from the measurements compares well with previous determinations derived from microwave and Doppler-limited far-infrared data. The observed quadrupole splittings in the sub-Doppler

data provide a signature to help confirm rotational assignments because the quadrupole patterns are distinctive to a given rotational quantum number change. All but one of the 50+ measurements show quadrupole hyperfine patterns that match those expected based on predictions from the known splittings in the lowest inversion doublet levels. The intriguing fact is that the perturbed rotational level $(4, 3)_a$ in the 1010(10) vibrational level with E' symmetry, lies just 1200 MHz⁷ above the $(5, 4)_s$ level of 1002(02) with A'_2 symmetry. For ammonia, ortho- proton nuclear spin wavefunctions have A'_1 symmetry while para- functions are E' .³ The Pauli exclusion principle requires that the overall molecular wavefunctions, including nuclear spin, have symmetry A'_2 or A''_2 for + or - parity. Hence the two levels in question belong to the para- and ortho- modifications of the molecule, respectively. This pair of levels is unique among the known levels of ammonia in this energy region in that they are close together and of the appropriate symmetries to be mixed.

Mechanisms for ortho-para mixing in molecules were first examined by Curl²⁰ and more recent relevant work has been reported.²¹⁻²³ For closed shell molecules, the interaction terms are small and near degeneracy between the mixed levels is needed. Spherical tops such as CH_4 ²⁴ and SF_6 ²⁵ posses level structure satisfying this condition and are the two examples exhibiting direct spectroscopic effects due to ortho-para mixing that have been reported. In other molecules including methyl fluoride,²⁶ formaldehyde²⁷ and ethylene²⁸ collisional interconversion has been reported. A report by Hepp *et al.*²⁹ noted an overpopulation in the $(J, K) = (1, 1)$ level in ammonia in spectra recorded following a supersonic expansion of a 10% sample of the gas in argon. The observation was rationalized by assuming that hard NH_3 dimer collisions permitted nuclear spin exchange. Spectra recorded at lower and higher seed gas concentrations did not show non-equilibrium ortho-para population distributions. There are no near-coincident ortho-para levels in the levels populated at ambient temperature²³ that could lead to nuclear spin exchange in the isolated molecule. The present observation would represent the first spectroscopic signature of the effects of ortho-para mixing in ammonia or indeed any non-spherical top closed shell molecule. In open shell molecules, the electron spin-nuclear spin hyperfine interaction results in much larger interaction terms and Tanaka *et al.*³⁰ have been recently discussed this situation in detail.

For the present, the size of the mixing term calculated by Cacciani *et al.* in ammonia²³ is too small to explain a perturbation of the size seen here for a pair levels that are 1200

MHz apart. However, it is clear that the observed $(4, 3)_a$ level in 1010(10) suffers an unusual perturbation affecting the quadrupole hyperfine structure that is not seen elsewhere in the data. We attempted to detect other transitions terminating in the same upper level, and in the putative perturbing one, but, due to frequency coverage limits of the extended cavity diode laser in the current version of the spectrometer, were unable to reach the frequencies required for the stronger ones, and could not detect saturation dips at the predicted positions of weaker transitions occurring at accessible frequencies. Clearly, the detection of spectroscopic transitions to confirm or deny the possibility of ortho-para mixing in these levels must be a future priority.

V. ACKNOWLEDGEMENTS

Work at Brookhaven National Laboratory was carried out under Contract No. DE-SC0012704 with the U.S. Department of Energy, Office of Science, and supported by its Division of Chemical Sciences, Geosciences and Biosciences within the Office of Basic Energy Sciences.

REFERENCES

- ¹H. W. Kroto, *Molecular Rotation Spectra* (Dover Publications, NY, 1992).
- ²C. H. Townes and A. L. Schawlow, *Microwave Spectroscopy* (Dover Publications, NY, 1975).
- ³P. R. Bunker and P. Jensen, *Molecular Symmetry and Spectroscopy, Second Edition* (NRC Press, Ottawa, 1998).
- ⁴K. Sung, L. R. Brown, X. Huang, D. W. Schwenke, T. J. Lee, S. L. Coy, and K. K. Lehmann, *J. Quant. Spectr. and Rad. Transf* **113**(11), 1066 (2012).
- ⁵P. Cacciani, P. Cermak, J. Cosléou, M. Khelkhal, P. Jeseck, and X. Michaut, *J. Quant. Spectr. and Rad. Transf* **113**, 1084 (2012).
- ⁶T. Foldes, D. Golebiowski, M. Herman, T. P. Softley, G. DiLonardo, and L. Fusina, *Molec. Phys.* **112**, 2407 (2014).
- ⁷A. R. AlDerzi, T. Furtenbacher, J. Tennyson, S. N. Yurchenko, and A. G. Császár, *J. Quant. Spectr. and Rad. Transf* **161**, 117 (2015).

⁸K. K. Lehmann and S. L. Coy, J. Chem. Soc., Faraday Trans. 2 **84**(9), 1389 (1988).

⁹A. E. Douglas and J. M. Hollas, Can. J. Phys. **39**(4), 479 (1961).

¹⁰A. Czajkowski, A. J. Alcock, J. E. Bernard, A. A. Madej, M. Corrigan, and S. Cheurov, Opt. Exp **17**, 9258 (2009).

¹¹G. Berden, R. Peeters, and G. Meijer, Chem. Phys. Letts. **307**, 131 (1999).

¹²R. Lees, L. Li, and L.-H. Xu, J. Mol. Spectrosc **251**, 241 (2008).

¹³S. G. Kukolich, Phys. Rev. **156**, 83 (1967).

¹⁴S. G. Kukolich, Phys. Rev. **172**, 59 (1967).

¹⁵S. G. Kukolich and S. C. Wofsy, J. Chem. Phys. **52**, 5477 (1970).

¹⁶J. T. Hougen, J. Chem. Phys. **57**, 4207 (1972).

¹⁷S. Twagirayezu, M. J. Cich, T. J. Sears, C. P. McRaven, and G. E. Hall, J. Molec. Spectrosc. **316**, 64 (2015).

¹⁸O. Axner, P. Kluczynski, and M. Lindberg, J. Quant. Spectr. and Rad. Transf. **68**, 299 (2001).

¹⁹Š. Urban, R. D'Cuhna, K. N. Rao, and D. Papoušek, J. Molec. Spectrosc. **62**, 1775 (1984).

²⁰R. F. Curl, J. V. V. Kasper, and K. P. Pitzer, J. Chem. Phys. **46**, 3220 (1967).

²¹P. L. Chapovsky, Phys. Rev. A **43**, 3624 (1991).

²²A. Miani and J. Tennyson, J. Chem. Phys. **120**, 2732 (2004).

²³P. Cacciani, J. Cosléou, M. Khelkhal, M. Tudorie, C. Puzzurini, and P. Pracna, Phys. Rev. A **80**, 042507(10) (2009).

²⁴L. Ozier, P. N. Yi, A. Khosa, and N. F. Ramsay, Phys. Rev. Letts. **24**, 642 (1970).

²⁵J. Bordé, C. J. Bordé, C. Salomon, A. Van Leberghe, M. Ouhayoun, and C. D. Cantrell, Phys. Rev. Letts. **45**, 14.

²⁶P. L. Chapovsky and L. J. F. Hermans, Annu. Rev. Phys. Chem. **50**, 315 (1999).

²⁷G. Peters and B. Schramm, Chem. Phys. Letts. **302**, 181 (1999).

²⁸Z.-D. Sun, K. Takagi, and F. Matsushima, Science **310**, 1938 (2005).

²⁹M. Hepp, G. Winnewisser, and K. M. T. Yamada, J. Molec. Spectrosc. **153**, 376 (1992).

³⁰K. Tanaka, K. Harad, and T. Oka, J. Phys. Chem. A **117**, 9584 (2013).

VI. FIGURES AND TABLES

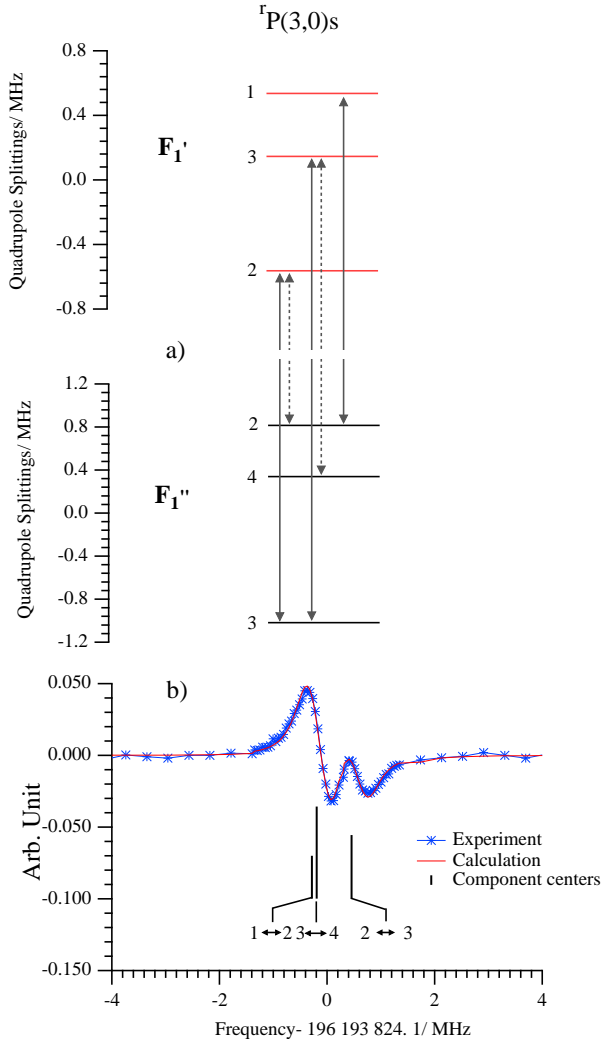


FIG. 1. Saturation dip line shape for $^rP(3,0)_s$ in the $v_1 + v_3$ band at 196 193.824 124(20) GHz, recorded at pressure of 5 mTorr and one way intracavity power of 100 mW. The upper panel shows the quadrupole splitting patterns for the levels labelled by the quantum number F_1 for the lower level (left) and upper level (right). The lower panel shows how the line shape arises from multiple quadrupole components. The vertical lines in the stick spectrum below the lower panel have heights proportional to the relative intensities of the three main ^{14}N hyperfine components with $\Delta F_1 = \Delta J$.

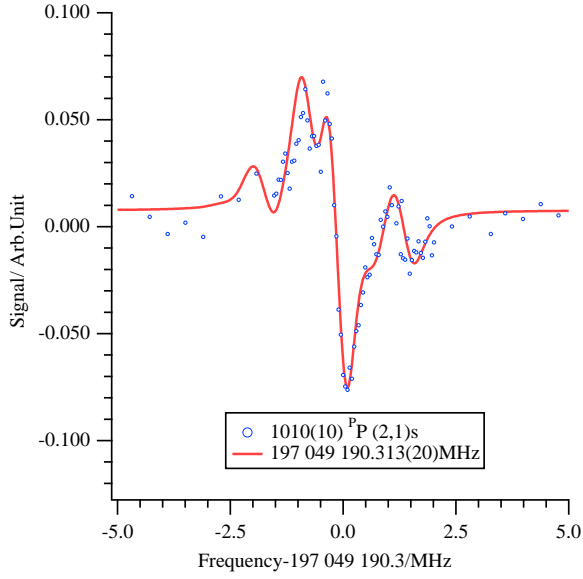


FIG. 2. $^pP(2,1)_s$ in the $v_1 + v_3$ band at 197 049.190 313(20) GHz. The dots are the experimental data and the solid line is the modeled line shape assuming the ground state quadrupole parameters do not change on excitation. The transition shows more complex hyperfine structure because the $\Delta F_1 \neq \Delta J$ components are relatively stronger compared to the $\Delta F_1 = \Delta J$ ones for lower- J transitions.

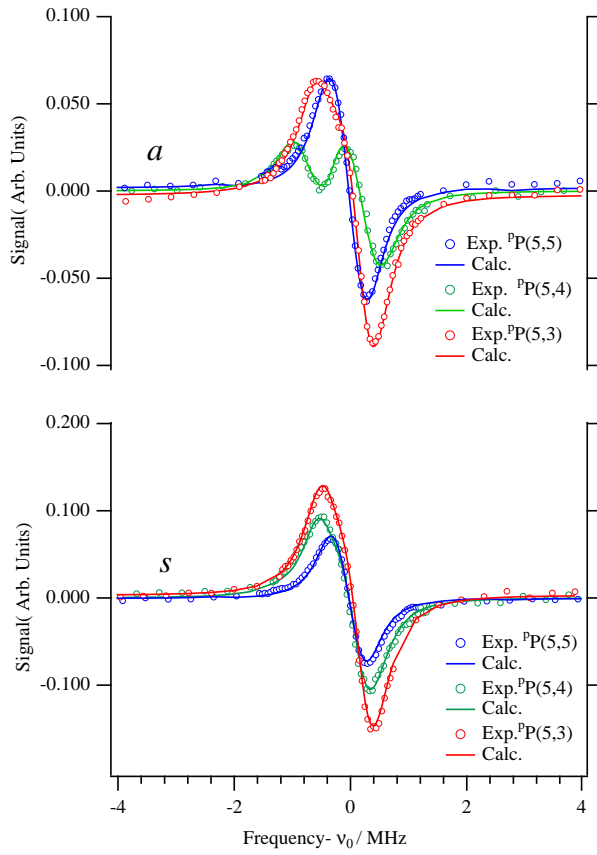


FIG. 3. Saturation dip line shapes for $P(5,3)$, $P(5,4)$ and $P(5,5)$ transitions showing distorted or split line shapes due to hyperfine effects. The $P(5,4)_a$ -component line is anomalous and deviates strongly from the line shape expected based on the known quadrupolar hyperfine parameters.

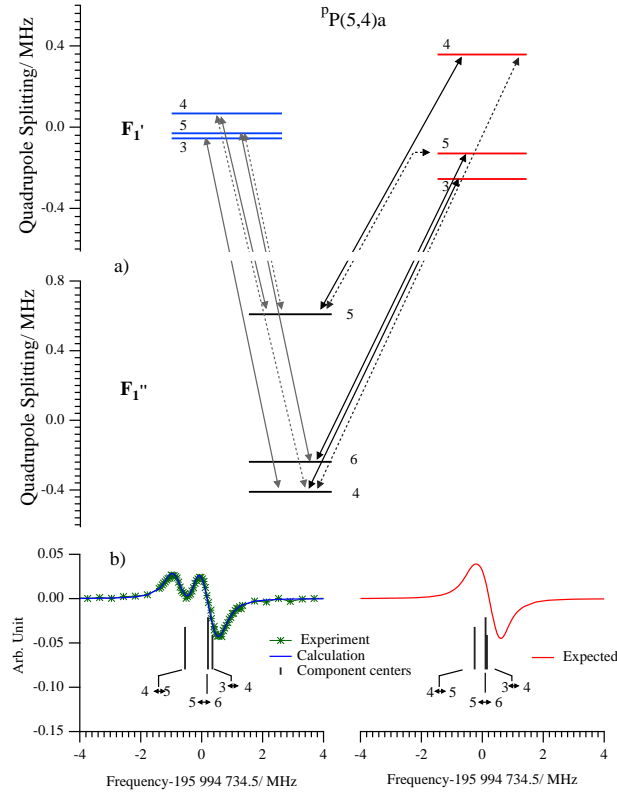


FIG. 4. Quadrupole energy patterns and line centers for the most intense quadrupole components of the $P(5,4)_a$ line showing the differences in the upper state quadrupole hyperfine splittings between the expected pattern (upper panel, right) and those needed to reproduce the observed pattern (left). The most intense quadrupole components are shown with solid line arrows, while the weaker $\Delta F_1 \neq \Delta J$ ones are shown with dotted lines.

TABLE I: Frequency measured lines in the near-infrared spectrum of ammonia

N'	K'	N''	K''	Vibration ^a	E''cm ⁻¹ ^b	Frequency/GHz ^c	cm ⁻¹	Previous/cm ⁻¹ ^d
3	2	4	3	0012(12)a	166.087889	198361.659685	6616.6327535	6616.633
3	2	4	3	0012(12)s	165.331083	198369.730830	6616.9019779	6616.902
4	4	5	5	0012(12)a	206.087431	198230.227211	6612.2486381	6612.249
4	4	5	5	0012(12)s	205.269098	198221.617673	6611.9614548	6611.962
6	4	7	5	0012(12)a	463.707007	194511.328210	6488.1995200	6488.200*
3	2	4	3	1002(02)a	166.087888	195073.628560	6506.9558408	6506.956
3	2	4	3	1002(02)s	165.331083	195113.933570	6508.3002712	6508.301
4	2	5	3	1002(02)a	265.226620	194549.591940 ^e	6489.4758607	6489.476
4	2	5	3	1002(02)s	264.516615	194558.668340 ^e	6489.7786168	6489.779
4	4	5	5	1002(02)a	206.087431	195165.624892	6510.0245081	6510.025
5	4	6	5	1002(02)a	325.127182	194607.591710 ^e	6491.4105247	6491.411
1	0	1	1	1010(10)a	16.963349	198243.691814 ^e	6612.6977689	6612.704*
1	0	1	1	1010(10)s	16.172993	198241.337160 ^e	6612.6192261	6612.619
1	0	2	1	1010(10)s	55.938722	197049.190313 ^e	6572.8534876	6572.854
2	0	2	1	1010(10)a	56.709214	198244.484501	6612.7242101	6612.726*
2	0	2	1	1010(10)s	55.938722	198244.855520	6612.7365859	6612.726*
2	0	3	1	1010(10)a	116.278269	196458.648780	6553.1551424	6553.155
2	1	3	0	1010(10)s	119.237839	196193.824124	6544.3215427	6544.322
3	0	3	1	1010(10)a	116.278269	198244.327123	6612.7189605	6612.726*
3	0	3	1	1010(10)s	115.536605	198247.689375	6612.8311131	6612.833*
3	0	4	1	1010(10)a	195.611277	195865.982837	6533.3859345	6533.386
3	0	4	1	1010(10)s	194.906311	195868.244853	6533.4613872	6533.461
3	1	4	0	1010(10)a	199.293900	195618.241805	6525.1221832	6525.122
3	1	4	2	1010(10)a	184.553024	196106.363145	6541.4041585	6541.405
3	1	4	2	1010(10)s	183.829075	196105.846984	6541.3869412	6541.387
3	2	3	1	1010(10)a	116.278269	197752.153450	6596.3018139	6596.302*
3	2	4	1	1010(10)a	195.611277	195373.809131	6516.9687868	6516.970
3	2	4	1	1010(10)s	194.906311	195375.305456	6517.0186989	6517.020
3	2	4	3	1010(10)a	166.087888	196328.038380	6548.7984484	6548.798
3	2	4	3	1010(10)s	165.331083	196322.408681	6548.6106619	6548.611
4	0	4	1	1010(10)a	195.611277	198242.993623	6612.6744797	6612.673*
4	0	4	1	1010(10)s	194.906311	198247.789736	6612.8344608	6612.824*
4	0	5	1	1010(10)a	294.629992	195274.486618	6513.6557444	6513.656
4	0	5	1	1010(10)s	293.968256	195277.986831	6513.7724989	6513.773
4	1	5	2	1010(10)a	283.616663	195531.648422	6522.2337388	6522.234
4	1	5	2	1010(10)s	282.937143	195523.772061	6521.9710117	6521.971
4	2	5	3	1010(10)a	265.226620	195727.557554	6528.7685641	6528.769
4	2	5	3	1010(10)s	264.516615	195740.182541	6529.1896883	6529.190
4	3	5	4	1010(10)a	239.408225	195994.734505	6537.6806279	6537.681
4	3	5	4	1010(10)s	238.652596	195962.122314	6536.5928023	6536.593
4	4	5	5	1010(10)a	206.087431	196136.937270	6542.4240015	6542.424
4	4	5	5	1010(10)s	205.269098	196142.933714	6542.6240214	6542.624
5	2	6	3	1010(10)a	383.977459	195171.619988	6510.2244830	6510.225

...continued on next page

TABLE I ...continued from previous page

N'	K'	N''	K''	Vibration ^a	E''cm ⁻¹ ^b	Frequency/GHz ^c	cm ⁻¹	Previous/cm ⁻¹ ^d
5	4	6	5	1010(10)a	325.127182	195560.864922	6523.2082964	6523.208
5	4	6	5	1010(10)s	324.368904	195583.055630	6523.9484987	6523.949*
5	5	6	6	1010(10)a	284.410125	195727.661582	6528.7720341	6528.772
5	5	6	6	1010(10)s	283.574345	195731.505651	6528.9002584	6528.901
6	0	6	1	1010(10)s	412.624301	198242.568537	6612.6603004	6612.653*
6	2	7	3	1010(10)a	522.222914	194500.699730	6487.8449921	6487.845
6	2	7	3	1010(10)s	521.621923	194570.952480	6490.1883716	6490.189
6	5	7	6	1010(10)s	422.458103	195194.649722	6510.9926722	6510.993
7	0	7	1	1010(10)s	550.758585	198257.822506	6613.1691180	6613.169

Footnotes:

- a.* Labels are the upper and lower level rotational quantum numbers, $v_1v_2v_3v_4(|l_3|, |l_4|)$ for the upper level in the transition and inversion symmetry (a or s) of the levels involved.
- b.* Lower state energy from Urban *et al.*¹⁹
- c.* Measured frequencies have an absolute error estimated to be less than 20 kHz unless indicated. See text for details. The corresponding wavenumbers are also given in the following column.
- d.* Previous measurements from Sung *et al.*⁴ and Földes *et al.*⁶ and references therein. Transitions marked with an asterisk are blended in the Doppler-limited spectrum.
- e.* Line center measurement less accurate due to poor signal-to-noise or complex hyperfine pattern. Estimated errors up to ± 30 kHz.

TABLE II. Calculated quadrupole splittings for rotational levels of NH₃ in kHz

J	K	F ₁ =J-1	F ₁ =J	F ₁ =J+1
1	0	2043.8	-1021.9	204.4
1	1	-1022.3	511.1	-102.2
2	0	1020.8	-1020.8	291.7
2	1	510.6	-510.6	145.9
2	2	-1022.4	1022.4	-292.1
3	0	815.4	-1019.3	339.8
3	1	611.8	-764.7	254.9
3	2	-0.0	0.0	-0.0
3	3	-1022.7	1278.4	-426.1
4	0	726.6	-1017.2	369.9
4	1	617.8	-864.9	314.5
4	2	291.1	-407.5	148.2
4	3	-255.1	357.2	-129.9
4	4	-1023.2	1432.5	-520.9
5	0	676.4	-1014.6	390.2
5	1	609.0	-913.4	351.3
5	2	406.4	-609.6	234.5
5	3	67.9	-101.8	39.2
5	4	-408.3	612.4	-235.5
5	5	-1024.0	1536.1	-590.8
6	0	643.6	-1011.4	404.6
6	1	597.9	-939.5	375.8
6	2	460.4	-723.5	289.4
6	3	230.6	-362.4	145.0
6	4	-92.5	145.4	-58.1
6	5	-510.5	802.1	-320.9
6	6	-1025.1	1610.8	-644.3
7	0	620.1	-1007.7	415.0
7	1	587.1	-954.1	392.9
7	2	488.0	-793.0	326.5
7	3	322.2	-523.6	215.6
7	4	89.1	-144.8	59.6
7	5	-212.4	345.1	-142.1
7	6	-583.7	948.5	-390.5
7	7	-1026.3	1667.8	-686.7

TABLE III. Ground state combination differences determined from the measurements

(J,K) - (J,K)	Frequency/GHz	Urban <i>et al.</i> ¹⁹
(2,1) - (1,1)s	1192.146847	1192.146564
(4,1) - (3,1)s	2379.444522	2379.443925
(4,1) - (3,1)a	2378.344319	2378.343747
(5,1) - (4,1)a	2968.507005	2968.506396
(5,1) - (4,1)s	2969.802905	2969.802399